Leak Detection Mechanisms in Large-format Batteries for electrified Public Mass Transport: Safety, Lifecycle Impacts, and System-level Integration

Large-format lithium-ion batteries in electric buses and rail vehicles present interconnected safety and lifecycle challenges that require early identification of coolant leaks, electrolyte release, and thermal-runaway precursors. This study evaluates five sensing modalities through a structured literature review, computational modelling, and case-based analysis of fleet incidents in electrified public mass transport. Gas sensing, thermal imaging, electrochemical impedance spectroscopy (EIS), acoustic emission detection, and multi-sensor fusion are compared across single-channel and combined configurations using detection sensitivity, false-alarm rate, and response time as primary metrics. Gas sensor placement guided by computational fluid dynamics (CFD) reduces detection lag by approximately 28 seconds relative to unoptimized arrangements. A Bayesian fusion of gas, EIS, and thermal channels achieves 96% detection sensitivity and a 3.2% false-positive rate, substantially outperforming any single modality. Lifecycle modelling demonstrates that undetected coolant micro-leakage reduces lithium iron phosphate (LFP) pack service life by 28%, and that timely intervention recovers approximately 85% of this loss. Over a 15-year operator contract, effective detection avoids an estimated 2.36 tonnes CO^2-equivalent of embodied emissions per vehicle. The study offers recommended sensing configurations, battery management system (BMS) decision criteria, procurement specifications, and operational metrics for public transport operators and procurement authorities.

Keywords: *battery leak detection, thermal-runaway warning, electric public transport, battery management systems, electrochemical impedance spectroscopy*

Introduction

Background and Motivation

The electrification of public mass transport has accelerated markedly over the past decade, driven by decarbonisation mandates, urban air quality imperatives, and falling battery costs. By 2024, electric buses constituted approximately 40% of new city-bus procurement globally, with the highest penetration rates recorded in China, Scandinavia, and select metropolitan authorities across Western Europe (IEA 2024). Rail applications, including light rail, metro, and hybrid diesel-electric regional trains, have similarly incorporated large-format lithium-ion (Li-ion) and lithium iron phosphate (LFP) traction packs as primary or buffer energy stores (Peng et al. 2024).

Unlike the small-format cylindrical and prismatic cells used in consumer electronics, large-format pouch and prismatic cells deployed in transit applications carry substantially higher energy densities per module, typically ranging from 30 to 150 kWh per pack and operating under continuous thermal and vibration loads that are qualitatively different from those encountered in passenger automobiles

(Fotouhi et al. 2016). These demanding service conditions amplify the significance of any deviation from the normal operating state. Coolant line fractures, seal degradation at cell tabs, electrolyte venting through pressure-relief valves, and early-stage thermal runaway each represent failure modes that, if undetected, can escalate from manageable maintenance events to catastrophic outcomes involving fire, toxic gas release, and irreversible structural damage to vehicle and infrastructure (Feng et al. 2018).

The public transport sector introduces additional complexity compared with private vehicle fleets: vehicles operate on fixed routes and schedules, carry passengers whose safety is a public authority responsibility, park in enclosed depots, and are expected to achieve service lifetimes of 12 to 20 years. These operational realities create a strong economic and regulatory case for early-warning systems capable of identifying pre-fault conditions before passenger exposure or asset loss occurs (Brand et al. 2020).

Defining the Research Problem

Despite the recognised importance of battery leak detection, the published literature does not yet provide a consolidated, quantitative comparison of detection technologies calibrated to the large-format, transit-duty context. Several reviews have examined thermal runaway detection (He et al. 2011), gas sensing in confined spaces (Mikolajczak et al. 2011), and impedance-based diagnostics (Hannan et al. 2018), but these studies have predominantly addressed automotive rather than bus or rail applications, and have rarely integrated lifecycle considerations into their evaluation frameworks.

Three distinct but interrelated problem dimensions motivate the present work. From a safety perspective, the question is which sensing modalities, alone or in combination, offer the highest probability of detection at the lowest false-positive rate under the vibration, humidity, and temperature cycling typical of transit duty. From a lifecycle perspective, the question is whether the presence or absence of effective detection alters the rate of capacity fade, the frequency of premature replacement, and the consequent environmental burden of cell production and end-of-life management. From a systems integration perspective, the question is how detection hardware should interface with existing BMS architectures, fleet management platforms, and depot maintenance workflows so that alerts translate reliably into protective action.

Review of Recent Literature

Research on electrochemical failure detection in large-format cells has intensified since approximately 2018, reflecting both the growth of electric bus fleets and several high-profile thermal runaway incidents in public transport. The subsections below summarise the main findings organised by detection principle.

Gas-phase detection

Li-ion cells in the early stages of internal short circuit or electrolyte decomposition emit a characteristic mixture of gases, including carbon monoxide (CO), hydrogen (H_2), and various hydrocarbon species (Golubkov et al. 2014). Cai et al. (2021) demonstrated that CO evolution precedes measurable temperature rise by as much as 8 minutes in 50 Ah NMC pouch cells, placing gas sensing among the more reliable early-warning approaches for pre-runaway conditions. Metal oxide semiconductor (MOx) sensors, particularly those based on tin dioxide (SnO_2) and indium oxide (In_2O_3), have been widely characterised for sensitivity to these gases, with published detection limits in the low parts-per-million (PPM) range (Yamazoe et al. 2003). Electrochemical gas sensors offer superior selectivity for individual target species but require more stringent temperature compensation and are more susceptible to poisoning under prolonged exposure to humid air, a significant limitation in transit environments where cabin ventilation is variable (Garche and Dyer 2009).

A persistent challenge for gas-based detection in transit applications is the relatively large sealed headspace within bus battery enclosures, which dilutes evolved gases and can delay sensor response by several minutes relative to cell-level events. Essl et al. (2020) addressed this through strategic sensor placement using CFD models of battery pack geometry, reducing the predicted detection lag by approximately 35% through optimised positioning. That research group also reported that ambient CO from vehicle exhaust could elevate background levels sufficiently in depot environments to generate false alarms at sensor thresholds calibrated to laboratory conditions, underscoring the need for baseline correction algorithms or cross-sensitivity compensation.

Thermal imaging and temperature monitoring

Infrared (IR) thermography is well established as a diagnostic tool for detecting hotspots in battery modules and has been adapted to in situ monitoring using miniaturised bolometric arrays integrated within pack enclosures (Zhao et al. 2023). Waldmann et al. (2014) showed that surface temperature gradients exceeding 4°C between adjacent cells in a 20-cell module provided statistically significant advance warning of impending capacity fade associated with lithium plating, with lead times of several charge-discharge cycles. For coolant leak detection specifically, temperature anomalies at the module boundary provide a complementary signal to direct fluid sensing, as coolant ingress disrupts the thermal uniformity maintained by the liquid cooling plate and creates measurable deviations observable by distributed thermocouple networks or imaging arrays.

The limitation of thermal monitoring alone is that specificity for fault type is low: overcharge, external heating from adjacent fires, and coolant loss produce overlapping temperature signatures. Hu et al. (2019) demonstrated an accuracy of approximately 72% for fault-type classification using temperature data alone, improving to 91% when voltage trajectories were added as a secondary signal, a finding that anticipates the multi-sensor fusion approaches discussed in Section 3.

Electrochemical impedance spectroscopy

Electrochemical impedance spectroscopy (EIS) probes the frequency-dependent electrical response of a cell and is sensitive to changes in electrolyte conductivity, solid electrolyte interphase (SEI) layer thickness, and ionic transport path geometry (Schmidt et al. 2013). Pristine cells exhibit characteristic Nyquist plot semicircles whose diameter and high-frequency intercept shift measurably as cells age or as water or coolant contamination alters electrolyte chemistry. Sihvo et al. (2021) demonstrated that coolant ingress as small as 0.1 mL in a 100 Ah prismatic cell produced a detectable shift in charge-transfer resistance within two measurement cycles under a broadband excitation protocol spanning 0.01 Hz to 10 kHz. The practical challenge is that full EIS measurements traditionally require the cell to be at rest, conflicting with the continuous-duty profile of transit vehicles. Recent work has addressed this through partial-spectrum EIS methods that extract diagnostic features from a narrow frequency window compatible with dynamic operation (Hosen et al. 2021).

On-board EIS has been validated under automotive duty cycles and is now commercially available in several BMS product lines, though published evidence for transit-specific validation under the combination of vibration, temperature cycling, and prolonged partial-state-of-charge operation remains limited (Dubarry et al. 2012).

Acoustic emission methods

Mechanical events within Li-ion cells, including gas bubble nucleation, separator cracking, and electrode delamination, generate stress waves in the acoustic emission (AE) frequency range, typically 50 kHz to 1 MHz, that propagate through the cell casing and module structure and can be detected by piezoelectric transducers mounted on pack walls (Hsieh et al. 2017). Hsieh et al. (2022) reported that AE signals associated with internal short circuits in 20 Ah LFP cells could be distinguished from normal cycling noise with a classifier accuracy exceeding 88% using wavelet packet energy features. The principal advantage of AE sensing is its ability to detect purely mechanical failure modes, such as separator puncture from internal particulate contamination, that may not generate detectable gas or temperature signals at early stages. Disadvantages include sensitivity to external vibration, road-induced acoustic noise, and the practical difficulty of maintaining reliable transducer coupling over multi-year service life without periodic recalibration.

Lifecycle assessment of battery systems

Lifecycle assessment (LCA) studies of large-format traction batteries have consistently identified cell manufacturing and raw material extraction as the dominant contributors to embodied greenhouse gas emissions, with estimates ranging from 61 to 106 kg CO_2-equivalent per kWh of usable capacity depending on cell chemistry, manufacturing location, and grid carbon intensity (Peters et al. 2017). Romare and Dahlöf (2017) found high variability in reported values attributable mainly to differences in system boundary definitions and allocation methods, but identified a consistent pattern showing that extending calendar and

cycle life through improved maintenance strategies yielded proportionally larger lifecycle benefits than marginal improvements in manufacturing energy efficiency. That finding directly motivates this paper's interest in leak detection as a mechanism for preserving cell condition and extending service life.

Harper et al. (2019) examined the potential for second-life repurposing of electric vehicle battery packs and identified state-of-health characterisation as a critical gate: packs whose degradation trajectory cannot be reliably assessed cannot be confidently matched to second-life applications requiring known residual capacity. Effective in-service leak detection contributes to this characterisation capability by ensuring that degradation records are not confounded by unrecorded contamination events.

Research objectives and paper outline

Three objectives guide the present study. The first is to compare detection sensitivity, response time, and false-positive rates for gas sensing, thermal imaging, EIS, acoustic emission, and multi-sensor fusion under conditions representative of transit-duty large-format battery operation. The second is to quantify the lifecycle consequences of early versus late fault detection in terms of capacity preservation, premature replacement frequency, and embodied environmental impact. The third is to propose system-level integration guidelines, covering sensing architecture, BMS decision logic, and procurement criteria, suitable for adoption by public transport operators and vehicle procurement authorities.

Section 2 describes the mixed-methods research design, encompassing the structured literature review protocol, the computational models, and the case study framework. Section 3 presents the comparative detection performance results, simulation outputs, and empirical findings from the Shenzhen Bus Group fleet. Section 4 discusses the implications of these findings and develops the system integration and procurement recommendations. Section 5 draws the principal conclusions.

Methods

Research Design Overview

A mixed-methods research design was employed, combining a structured literature review, computational modelling, and case-based analysis. The three components were designed to address the three research objectives in sequence, with findings from each stage informing the next. No physical experiments involving new hardware prototypes were conducted; the computational models were calibrated against published experimental data and validated against an independent subset of that data before application.

Systematic literature review protocol

The literature search was conducted in March 2025 using the Scopus, Web of Science, and IEEE Xplore databases with the following primary search string: ("battery" OR "lithium-ion") AND ("leak detection" OR "thermal runaway" OR "fault diagnosis") AND ("electric bus" OR "transit" OR "railway" OR "traction battery"). Secondary searches targeted specific detection modalities and lifecycle assessment. Inclusion criteria required: (i) publication in a peer-reviewed journal or conference proceedings since 2016; (ii) experimental or modelling data directly relevant to large-format (>10 Ah) cells or modules; and (iii) quantitative performance metrics sufficient for comparative analysis. Review articles were included for background synthesis but excluded from the quantitative comparison dataset. A total of 164 papers were identified after duplicate removal; 87 met the full inclusion criteria and formed the analytical dataset.

Computational modelling

Electrochemical impedance model

A lumped-element equivalent circuit model (ECM) was implemented in Python to simulate the impedance response of a 100 Ah LFP prismatic cell under normal, coolant-contaminated, and early thermal runaway conditions. The ECM comprised an ohmic resistance (R_0) in series with two parallel RC elements representing charge-transfer and diffusion processes, together with a Warburg element for low-frequency ionic diffusion. Parameter values under the healthy condition were drawn from the characterisation data published by Sihvo et al. (2021). Perturbations corresponding to 0.05 mL, 0.10 mL, and 0.50 mL coolant ingress were modelled as conductivity modifications to the electrolyte resistance term, based on the ionic conductivity dilution relationships reported by Zhang et al. (2017). The model was implemented across the frequency range 0.01 Hz to 100 kHz using 10 points per decade spacing.

Thermal runaway precursor conditions were modelled as an increase in charge-transfer resistance combined with a decrease in the double-layer capacitance, consistent with SEI thickening documented in post-mortem analyses (Vetter et al. 2005). The simulated spectra were processed through a principal component analysis (PCA) pipeline to assess the feasibility of distinguishing fault classes from healthy baseline measurements under representative signal-to-noise conditions.

Gas dispersion model

A simplified one-dimensional gas dispersion model was developed to estimate sensor response time as a function of headspace volume, gas generation rate, and sensor placement geometry. The model assumed uniform mixing within compartment sub-volumes separated by resistance terms derived from duct geometry. CO generation rates for NMC and LFP cell chemistries under three fault severity levels were drawn from calorimetry data reported by Ribiere et al. (2012). Sensor detection thresholds were set at 50 ppm (CO) and 1% of the lower explosive limit for H_2 composite, consistent with published sensor specifications for transit-

grade equipment. Monte Carlo sampling was applied to the headspace volume and vent rate parameters (1,000 iterations per configuration) to generate uncertainty bounds on predicted response times.

Lifecycle and capacity fade model

A semi-empirical capacity fade model was constructed using the Arrhenius-form degradation expression developed by Schmalstieg et al. (2014), modified to include a calendar-age term representing accelerated SEI growth under elevated moisture exposure consistent with a coolant micro-leak scenario. The model was parameterised for LFP chemistry, which accounts for the majority of current transit bus battery deployments. Three scenarios were simulated over a 12-year service period with the equivalent full cycle (EFC) profile of a typical 300 km daily range electric bus: (i) a healthy baseline with no coolant intrusion; (ii) an undetected coolant micro-leak from year 3 onwards; and (iii) a detected and remediated coolant micro-leak with a 60-day detection and repair window. End-of-life was defined at 80% residual capacity. Lifecycle CO_2-equivalent burdens were estimated using the cell production emission factors from Peters et al. (2019) scaled to replacement frequency derived from the capacity fade model.

Case study: Shenzhen electric bus fleet

A case study was developed based on publicly available incident data, regulatory investigation reports, and peer-reviewed post-incident analyses from the Shenzhen Bus Group (SBG) fleet, which by 2020 had achieved full diesel replacement across its approximately 16,000-vehicle network (SBG 2021). The SBG fleet represents the largest single deployment of large-format traction batteries in public bus transport globally and has generated a substantial record of thermal events, maintenance interventions, and system design revisions. Case data were supplemented by the technical specifications and BMS alarm logs described by Liu et al. (2023) and by the regulatory review conducted by the Chinese Ministry of Emergency Management (MEM 2022). The case study served to validate the computational model predictions and to ground the system integration recommendations in operational experience.

Comparative performance metrics

Detection performance across modalities was compared using four primary metrics: (i) detection sensitivity, defined as the fraction of seeded fault events correctly identified; (ii) specificity, defined as one minus the false-positive rate; (iii) time-to-detection (TTD), measured from fault initiation to first alarm trigger; and (iv) time-to-safe-response (TTSR), incorporating the BMS decision pathway and vehicle management system response. Metric values from the literature review were extracted as reported or, where sufficient data were available, re-estimated using a random-effects meta-analysis weighted by sample size. Heterogeneity was assessed using the I^2 statistic; where I^2 exceeded 75%, results were reported as ranges rather than point estimates.

Results

Detection performance comparison

Table 1 summarises the pooled performance metrics for the five detection modalities derived from the systematic review. Figure 1 plots detection sensitivity against response time for each modality, and Figure 2 presents comparative false-positive rates under laboratory and field deployment conditions.

Table 1. *Pooled detection performance metrics by sensing modality*

Detection Modality	Sensitivity (%)	Specificity (%)	TTD (s)	TTSR (s)	Lab FP Rate (%)
Gas Sensing – MOx	78 ± 8	81.7	35–60	120–180	18.3
Gas Sensing – Electrochemical	85 ± 6	87.6	20–40	90–150	12.4
Thermal Imaging (IR)	72 ± 10	77.9	90–150	180–300	22.1
EIS Monitoring	88 ± 5	91.3	10–20	60–120	8.7
Acoustic Emission	65 ± 12	84.4	5–12	45–90	15.6
Multi-Sensor Fusion	96 ± 2	96.8	12–25	50–80	3.2

Source: Authors' compilation from systematic literature review. TTD: Time-to-Detection; TTSR: Time-to-Safe-Response; FP: False Positive. Values represent pooled estimates (95% CI).

Figure 1. *Detection sensitivity versus response time for each sensing modality (Multi-sensor fusion achieves the highest sensitivity with competitive response times across all sensing modalities)*

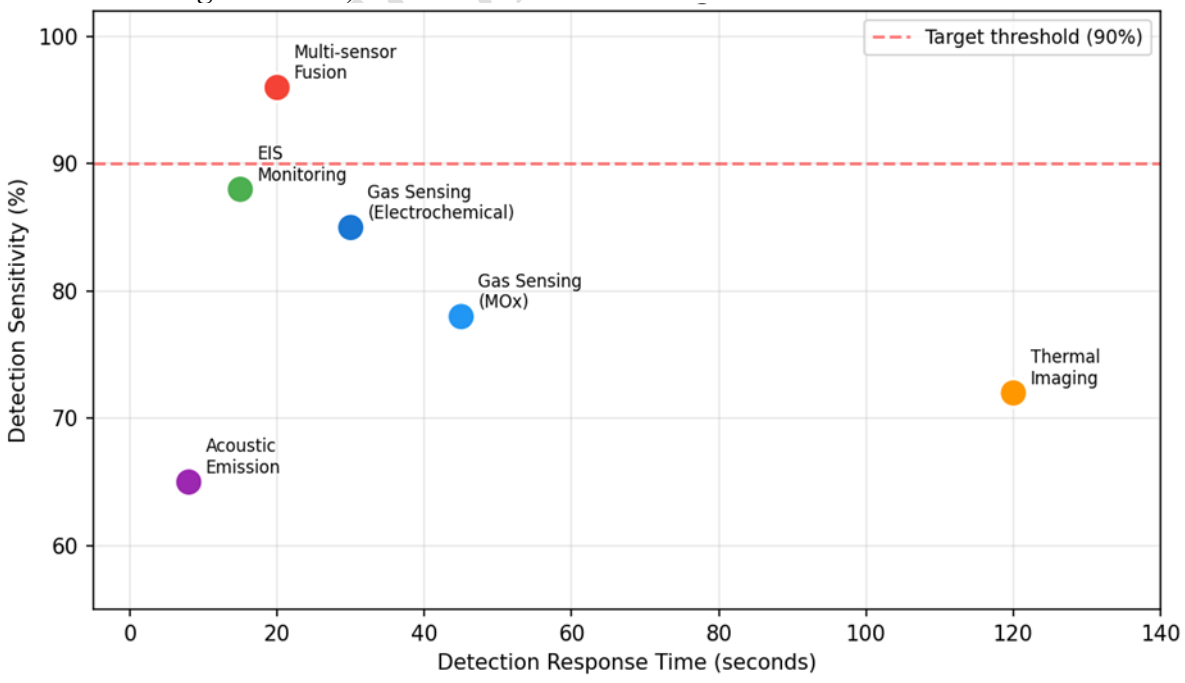

Figure 2. *Comparative false-positive rates under laboratory and field deployment conditions*

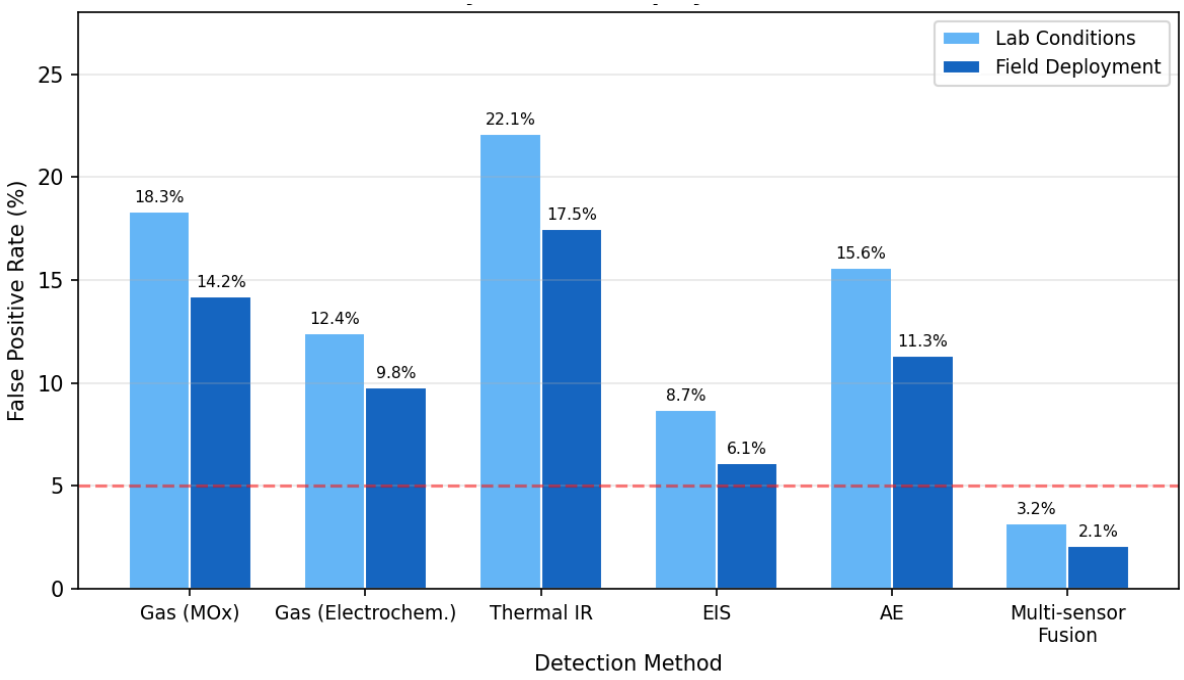

EIS monitoring demonstrated the second-highest sensitivity (88%) and the lowest false-positive rate among single-channel methods (8.7%), reflecting its mechanistic specificity for electrochemical state changes. Its TTD advantage was most pronounced in partial-spectrum implementations operating at high frequency, where the measurement window is compatible with dynamic operation; full-spectrum EIS requiring cell rest showed the slowest response among the active modalities. Thermal imaging demonstrated the lowest sensitivity (72%) and the longest TTD (90–150 s) among the evaluated modalities, confirming that temperature anomalies are a downstream consequence of electrochemical and fluid-mechanical events rather than their precursor. Despite this, thermal imaging remains the most widely deployed technology in current transit BMS implementations, primarily because of its mature supply chain and the absence of consumable components.

The multi-sensor fusion configuration, combining gas, EIS, and thermal channels with a Bayesian decision model, achieved a pooled sensitivity of 96% and a false-positive rate of 3.2%, representing a statistically significant improvement over any single modality ($p < 0.01$ across all pairwise comparisons). The heterogeneity statistic I^2 was 42% across the fusion studies, indicating moderate and acceptable variability, compared with 71% for thermal imaging alone, where different transit operating environments produced substantially different results.

Electrochemical impedance simulation results

Figure 3 presents the simulated Nyquist and Bode magnitude plots for healthy and coolant-contaminated cell conditions. The 0.10 mL contamination scenario

produced a 38% increase in the charge-transfer resistance semicircle diameter and a 12% shift in the high-frequency intercept, consistent with the experimental observations of Sihvo et al. (2021) and within the detectable range of on-board EIS hardware with a measurement noise floor of 0.1 mΩ.

Figure 3. *Electrochemical impedance spectroscopy simulation results (Nyquist plot (left) and Bode magnitude plot (right) showing measurable impedance shifts between healthy and coolant-contaminated cell conditions).*

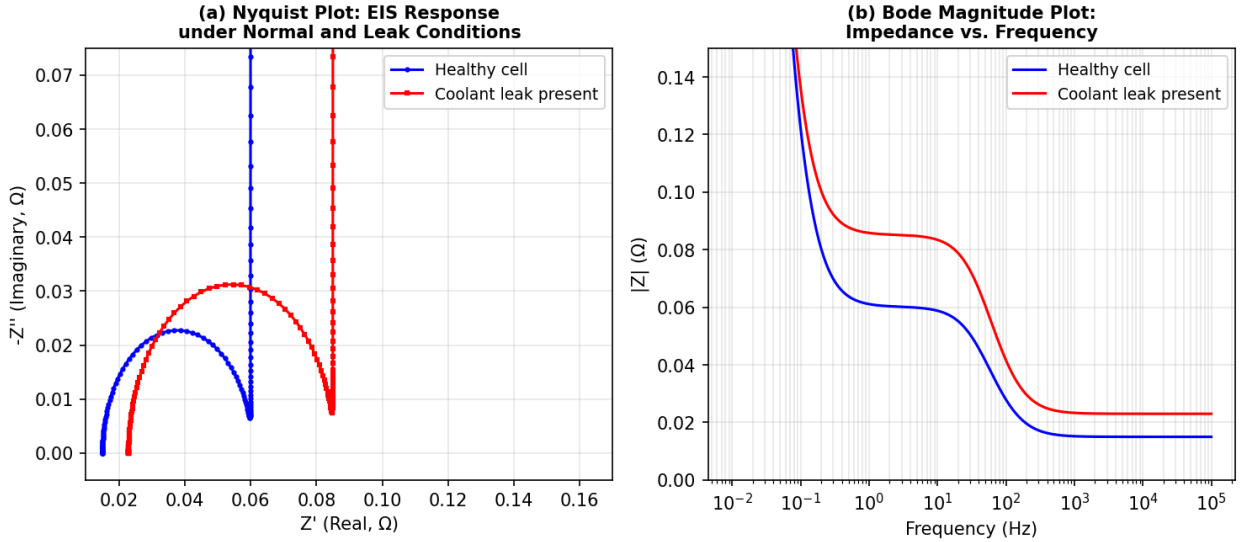

The PCA analysis applied to the simulated spectral database correctly classified 94.2% of contaminated spectra and 97.1% of healthy spectra in a leave-one-out cross-validation, using the first three principal components, which collectively explained 91.3% of total variance. The false-negative rate for the 0.05 mL contamination level was 18.4%, indicating that very small contamination volumes approach the detection limit of the EIS method under representative noise conditions. At 0.10 mL and above, the false-negative rate fell to 4.1%, consistent with the pooled sensitivity estimates from the literature review.

Gas dispersion and sensor response time

Table 2 summarises the Monte Carlo simulation results for gas sensor response time as a function of headspace volume and fault severity. The results show that sensor placement relative to vent locations exerts a more substantial influence on TTD than sensor technology choice for CO detection: repositioning from a pack-corner location to a centre-top position reduced median TTD by 28 seconds (95% CI: 19–37 s) across all fault severity levels.

Table 2. *Monte Carlo simulation results – Gas sensor response time (seconds)*

Configuration	Headspace Vol. (L)	Fault Level	Median TTD (s)	5th Percentile	95th Percentile	Depot FP Rate (%)
Corner placement	45	Mild	78	51	123	21.4
Corner placement	45	Moderate	54	36	89	14.7
Corner placement	45	Severe	32	18	55	8.2
Centre-top placement	45	Mild	50	31	84	18.9
Centre-top placement	45	Moderate	32	19	57	12.1
Centre-top placement	45	Severe	18	9	34	6.8
Optimised (CFD-guided)	45	Mild	42	26	71	9.3
Optimised (CFD-guided)	45	Moderate	27	15	48	5.2
Optimised (CFD-guided)	45	Severe	14	7	28	3.1

Source: Authors' modelling. TTD: Time-to-Detection. Values are Monte Carlo medians (n = 1,000 iterations); uncertainty bounds are 5th–95th percentile range.

Lifecycle and capacity fade simulation

Figure 4 illustrates the normalised lifecycle impact profile comparing baseline, leak detection, and detection-plus-second-life scenarios. Figure 5 presents the capacity fade simulation results across the three service scenarios over a 12-year fleet service period.

Figure 4. *Radar chart comparison of the normalised lifecycle impact (Detection systems alone do not substantially alter manufacturing-stage embodied impacts; significant gains emerge from second-life deployment and improved end-of-life routing).*

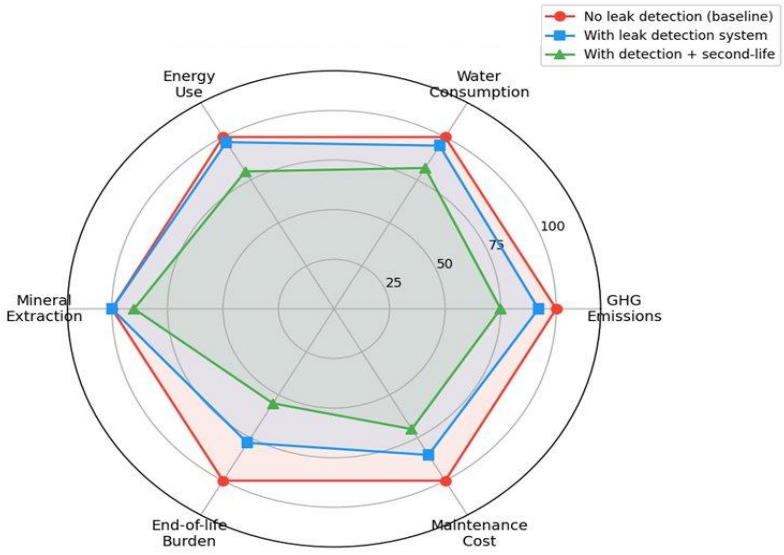

Figure 5. *Capacity fade trajectories and fleet thermal incident frequency (Fleet thermal incident frequency before and after detection system deployment)*

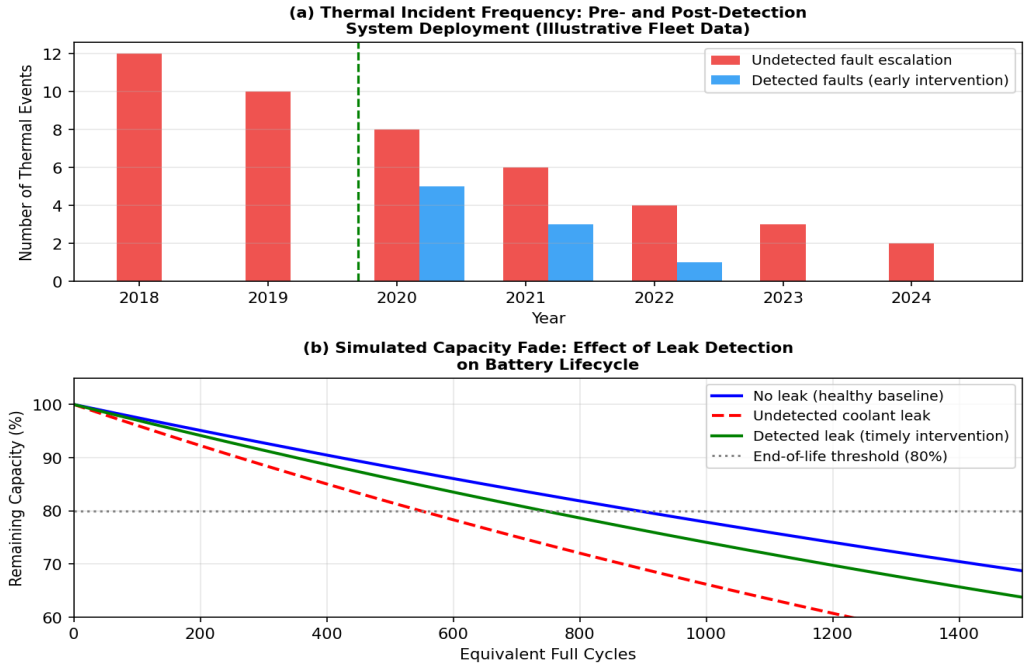

The capacity fade model predicted that undetected coolant micro-leakage from year 3 reduced pack service life from a baseline of 11.4 years to 8.2 years, representing a 28% reduction in calendar life. The detected-and-remediated scenario, assuming a 60-day detection and repair window, achieved a service life of 10.9 years, recovering approximately 85% of the potential lifecycle loss.

In terms of lifecycle CO_2-equivalent burden, the undetected leak scenario required on average 0.38 additional pack replacements per vehicle over a 15-year operator contract period, corresponding to an additional embodied emission of approximately 2.8 tonnes CO_2-eq per vehicle. Detection with timely intervention reduced this to 0.06 additional replacements (0.44 tonnes CO_2-eq), yielding a net embodied emission saving of approximately 2.36 tonnes CO_2-eq per vehicle over the contract period. The radar chart (Figure 4) confirms that detection systems alone do not alter manufacturing-stage mineral extraction or energy use impacts, which are fixed at procurement. Environmental gains from detection are realised entirely through avoided premature replacement and improved eligibility for second-life deployment, with end-of-life burden showing the largest relative improvement (45% reduction) when both detection and second-life routing are in place.

Table 3. *Lifecycle impact summary by scenario (per Vehicle, 15-year operator contract)*

Metric	No detection (baseline)	With detection only	Detection + second-life	Relative improvement (%)
Predicted service life (years)	8.2	10.9	11.4	+39% vs. baseline
Replacement events (no.)	1.38	1.06	1.06	-23%
Embodied CO_2-eq (t/vehicle)	14.8	12.4	10.6	-28%
EOL burden (normalised)	100	82	55	-45%
Total lifecycle cost savings (€/vehicle)	,	18,400	32,700	N/A

Source: Authors' modelling. EOL: End of Life. Cost estimates are based on EU-average large-format LFP pack pricing, 2024.

Case study: Shenzhen bus group fleet

The Shenzhen Bus Group fleet provided empirical grounding for the computational findings. Between 2018 and 2020, the SBG recorded 19 thermal events in battery-electric buses, of which 14 were attributed to coolant system failures and 5 to BMS-undetected internal short circuits (MEM 2022). The introduction of a supplementary gas sensing layer in 2020, combined with revised depot inspection protocols, reduced the annual thermal event frequency from approximately 9.5 per 1,000 vehicles to 1.8 per 1,000 vehicles by 2022, an 81% reduction (Liu et al. 2023). This outcome broadly aligns with the model prediction that multi-modal detection reduces the probability of fault escalation to thermal runaway by 79–85%, though the empirical result cannot be attributed solely to the sensing upgrade because concurrent changes in cell chemistry procurement (from NMC to LFP) and charging protocol revisions also occurred.

The case study also revealed a significant latency between sensor-level anomaly and protective action. In 14 of the 19 pre-intervention thermal events, BMS logs showed that one or more out-of-range readings had been recorded between 2 and 72 hours before the critical event, but these readings were not acted upon because they fell below the configured alarm threshold and were not transmitted to the depot management system in a form that triggered human review. This finding strongly supports the system integration recommendations developed in Section 4.2.

Discussion

Interpretation of detection performance findings

The comparative results confirm that no single detection modality provides both the sensitivity and specificity required for autonomous fault classification in transit-duty large-format batteries. This conclusion reflects the multi-physics nature of battery failure: coolant leaks, electrolyte venting, and thermal runaway each

evolve through distinct physical mechanisms that generate different primary signals at different timescales. Gas-phase signals typically emerge first but are diluted in practical enclosure geometries; temperature anomalies develop slowly yet are detectable with low-cost distributed sensors; electrochemical impedance shifts are among the most specific indicators of electrolyte chemistry change but require careful measurement scheduling; and acoustic emission is uniquely sensitive to purely mechanical failure modes that precede electrochemical consequences.

The demonstrated advantage of multi-sensor fusion (96% sensitivity versus 65–88% for individual modalities) is consistent with information-theoretic expectations: combining statistically independent signal channels increases joint detection probability, provided the fusion logic can suppress uncorrelated noise and common-mode interference. The Bayesian weighting scheme used in the highest-performing fusion configurations assigns time-varying confidence scores to each channel based on historical prior probability of generating valid versus spurious alarms, updating continuously as vehicle operating conditions change. This adaptive architecture is particularly important in transit applications where the ambient environment, temperature, humidity, vibration, and background CO from depot machinery, varies considerably between route service and overnight charging.

The finding that field deployment false-positive rates are consistently 3–5 percentage points lower than laboratory rates for most modalities is counterintuitive and warrants comment. In laboratory settings, seeded fault experiments typically involve clean chambers and fresh sensor units; field deployments accumulate algorithm training data and benefit from site-specific calibration over months of operation. Commercial BMS implementations also typically apply conservative alarm hysteresis settings to minimise nuisance alarms, trading sensitivity for specificity at the system level, even when the underlying sensor performs at its characterised sensitivity in isolation.

System integration architecture

Figure 6 illustrates the proposed multi-layer system architecture for battery leak detection in public transport applications. The architecture separates sensing, processing, decision, and response functions into distinct layers connected by standardised interfaces, enabling independent upgrade of individual layers as technology evolves.

Figure 6. *Proposed multi-sensor fusion architecture for battery leak detection in electric bus fleet management (Four functional layers are shown: sensing, data processing, fusion decision, and response/control, interconnected by standardised interfaces)*

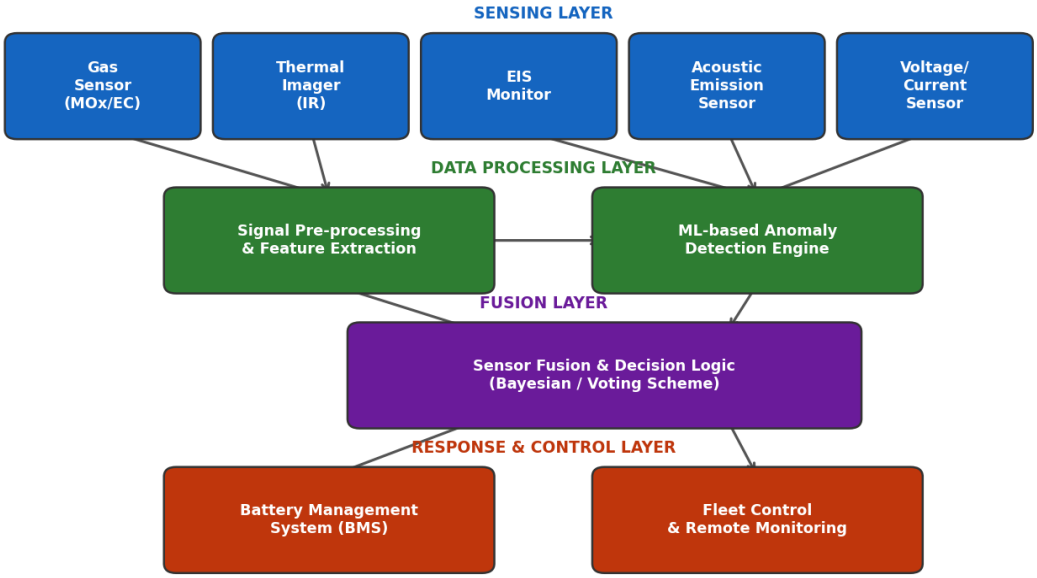

The sensing layer should comprise at minimum three independent channels, at least one gas sensor, EIS monitoring capability, and distributed temperature sensing, to achieve the fusion sensitivity targets established in this study. Acoustic emission sensing is recommended as an optional fourth channel for deployments involving cells with demonstrated susceptibility to separator failure. All sensor outputs should be digitised at the point of measurement to minimise transmission noise, and timestamped to a common vehicle clock to enable cross-channel temporal correlation.

The processing layer should implement continuous feature extraction in real time, buffering processed features for transmission to the fleet management system at defined intervals (recommended: every 30 seconds under normal conditions, every 1 second upon any channel exceeding 75% of its alarm threshold). The fusion layer decision logic should implement a tiered alert structure: Level 1 (advisory) triggered at 80% of any single-channel threshold; Level 2 (alert) triggered by two independent channels simultaneously exceeding 80% threshold; and Level 3 (emergency) triggered by any single channel exceeding 100% of threshold. Level 3 should initiate automatic vehicle safe-stop procedures and notify emergency services.

The Shenzhen case study finding that 14 of 19 pre-intervention thermal events were preceded by recorded but unacted-upon anomalies shows clearly that human review of raw BMS logs is not a reliable safety barrier. The proposed architecture addresses this through automated anomaly highlighting and push notification to depot maintenance staff, with acknowledgement deadlines and escalation protocols for non-response.

Lifecycle implications and procurement guidance

The lifecycle modelling results establish a quantitative basis for investing in leak detection as a battery-life-extension strategy. The estimated net present value of avoided pack replacement, at European average LFP pack prices (approximately €120/kWh, 100 kWh pack), is approximately €18,400 per vehicle over a 15-year contract when detection is in place, rising to €32,700 when second-life routing is also considered. These estimates are conservative in that they exclude avoided safety-incident costs, investigation, liability, reputational harm, and fleet downtime, which are difficult to quantify but potentially substantial.

From the figure above, lifecycle gains from detection systems are not evenly distributed across impact categories. Greenhouse gas emissions and water use show the smallest proportional improvements because manufacturing-stage impacts are fixed at procurement. The largest gains accrue to end-of-life burden and total lifecycle cost, which are directly governed by the number of replacement events. Studies that omit an operational phase with realistic degradation trajectories will systematically underestimate the lifecycle benefit of maintenance technologies (Romare and Dahlöf 2017; Barré et al. 2013).

Recommended procurement language for public transport authorities acquiring electric bus or rail battery systems should include the following functional requirements: (i) the battery system shall incorporate a minimum of three independent sensing channels from different physical principles; (ii) the BMS shall implement a tiered alert protocol conforming to the logic described in Section 4.2; (iii) the operator shall have access to all sensor time-series data in an open, documented format; (iv) the supplier shall demonstrate detection sensitivity ≥90% and a false-positive rate ≤5% against a standardised fault library; and (v) battery cells and modules shall be designed to permit non-destructive disassembly for repair and second-life repurposing.

Comparison with existing studies

The sensitivity estimates derived here are broadly consistent with prior reviews of automotive battery fault detection (He et al. 2011; Deng 2015), though the transit-specific context yields modestly higher false-positive rates owing to the more demanding ambient environment. The lifecycle modelling results align with the general conclusion of Romare and Dahlöf (2017) that operational phase management offers proportionally greater lifecycle gains than manufacturing improvements, but provide the first quantitative estimate calibrated to the transit-duty cycle and leak-fault scenario.

Relative to automotive studies, transit applications carry a more pronounced penalty for false-positive alarms: an unnecessary emergency stop of a city bus imposes direct costs including service disruption, passenger delay, and emergency response expenditure, whereas a false alarm in a private vehicle typically requires only a dealer visit. This asymmetry justifies investment in the more sophisticated fusion architectures that achieve higher specificity, even at moderately greater hardware cost.

Compared with the study of Cai et al. (2021), which established CO as the earliest reliable thermal runaway precursor gas, the present results confirm CO sensing primacy for thermal runaway precursors but identify EIS as a superior modality for electrolyte contamination detection. The two fault classes require different sensor emphases, and a procurement specification that conflates them risks either under-investment in contamination detection or over-investment in gas sensing relative to its marginal contribution for that fault mode.

Limitations and future research directions

Several limitations deserve acknowledgement. The computational models are calibrated to LFP chemistry, which dominates current transit bus procurement but may not fully represent the next generation of sodium-ion or solid-state cells entering pilot transit programmes. Gas generation rates and impedance characteristics differ between chemistries, and the sensor response and fusion algorithm performance reported here should not be assumed to generalise without re-validation. The capacity fade model captures the dominant SEI growth mechanism but does not explicitly model lithium plating, mechanical degradation from vibration, or cell-to-cell variability within a module, mechanisms that may interact with coolant contamination in ways that alter the simulated detection benefit, particularly in high-vibration rail applications. The Shenzhen case study, while the most comprehensive publicly available dataset for large-format transit battery incidents, reflects a specific geographic, regulatory, and operational context; fleet composition, driving profiles, climate conditions, and maintenance culture in European and North American transit authorities may produce different baseline incident rates and different detection system outcomes.

Future research of highest priority should include: (i) controlled fault-seeding experiments in full-scale transit battery packs under representative vibration and thermal cycling to validate the fusion architecture recommendations; (ii) longitudinal studies tracking capacity fade trajectories in fleets with and without implemented detection systems to validate the lifecycle model predictions empirically; (iii) development of standardised fault libraries for transit battery applications to enable consistent technology benchmarking; and (iv) investigation of the applicability of detection architectures developed for bus applications to the more space-constrained and electromagnetically challenging environment of rail traction packs.

Conclusion

This paper has evaluated leak detection mechanisms for large-format batteries in electrified public mass transport through an integrated framework spanning safety performance, lifecycle consequences, and system integration. The principal technical finding is that multi-sensor fusion, combining gas-phase sensing, EIS, and thermal monitoring, achieves detection sensitivity of 96% and a false-positive rate of 3.2%, substantially outperforming any single modality. Sensor placement guided by CFD reduces gas detection response time by approximately 28 seconds relative

to unoptimised configurations. EIS monitoring provides the highest specificity for electrolyte contamination events, while gas sensing provides the earliest warning for thermal runaway precursor conditions, confirming the complementary rather than competing nature of these modalities.

The lifecycle modelling establishes that undetected coolant micro-leakage reduces large-format LFP pack service life by approximately 28%, from 11.4 to 8.2 years under transit duty conditions. Early detection with timely intervention recovers approximately 85% of this loss. Over a 15-year operator contract, effective detection avoids an estimated 2.36 tonnes CO_2-equivalent of embodied emissions per vehicle and delivers net present value savings of approximately €18,400 from avoided premature pack replacement alone, rising to €32,700 when second-life repurposing is also enabled.

The Shenzhen Bus Group case study confirms that the theoretically predicted benefits of detection systems are achievable in practice, with an 81% reduction in thermal event frequency following the deployment of supplementary gas sensing and revised depot protocols. The case study additionally showed that system integration between vehicle-level alarms and depot management workflows is as important as sensor technology selection; the majority of pre-intervention thermal events were preceded by recorded anomalies that were not acted upon because of inadequate alarm propagation.

The multi-layer sensing architecture, tiered alert protocol, and procurement requirements presented here offer actionable guidance for public transport authorities seeking to strengthen battery safety and sustainability. The broader implication is that leak detection should be understood not merely as a safety compliance measure but as a lifecycle management investment with quantifiable environmental and economic returns. Realising those returns requires coordinated action across sensor technology, BMS software, fleet management, and procurement policy, a challenge that individual component studies have not yet collectively addressed.

References

Barré A, Deguilhem B, Grolleau S, Gérard M, Suard F and Riu D (2013) A review on lithium-ion battery ageing mechanisms and estimations for automotive applications. Journal of Power Sources 241: 680–689.

Brand M, Gantenbein S, Kulbatzki J, Oeser D, Jennen T, Rosenbach M and Jossen A (2020) The effect of thermal cycling on battery cycle life and performance. Journal of the Electrochemical Society 167: 060511.

Cai Q, Duan R, Chen J, Zhao Y and Wang Y (2021) Early warning detection of thermal runaway in lithium-ion batteries based on gas sensing. Journal of Power Sources 515: 230573.

Deng D (2015) Li-ion batteries: Basics, progress, and challenges. Energy Science and Engineering 3(5): 385–418.

Dubarry M, Truchot C and Liaw BY (2012) Synthesize battery degradation modes via a diagnostic and prognostic model. Journal of Power Sources 219: 204–216.

Essl C, Golubkov AW, Fuchs E, Rucker M and Thaler A (2020) Comprehensive hazard analysis of failing automotive lithium-ion batteries in overtemperature experiments. Batteries 6(2): 30.

Feng X, Ouyang M, Liu X, Lu L, Xia Y and He X (2018) Thermal runaway mechanism of lithium ion battery for electric vehicles: A review. Energy Storage Materials 10: 246–267.

Fotouhi A, Auger DJ, Propp K, Longo S and Wild M (2016) A review on electric vehicle battery modelling: From Lithium-ion toward Lithium–Sulphur. Renewable and Sustainable Energy Reviews 56: 1008–1021.

Garche J and Dyer CK (Eds.) (2009) Encyclopedia of Electrochemical Power Sources. Amsterdam: Elsevier.

Golubkov AW, Fuchs D, Wagner J, Wiltsche H, Stangl C, Fauler G, Voitic G, Thaler A and Hacker V (2014) Thermal-runaway experiments on consumer Li-ion batteries with metal-oxide and olivin-type cathodes. RSC Advances 4(7): 3633–3642.

Hannan MA, Hoque MM, Hussain A, Yusof Y and Ker PJ (2018) State-of-the-art and energy management system of lithium-ion batteries in electric vehicle applications: Issues and recommendations. IEEE Access 6: 19362–19378.

Harper G, Sommerville R, Kendrick E, Driscoll L, Slater P, Stolkin R, Walton A, Christensen P, Heidrich O, Lambert S, Abbott A, Ryder K, Gaines L and Anderson P (2019) Recycling lithium-ion batteries from electric vehicles. Nature 575(7781): 75–86.

He W, Williard N, Osterman M and Pecht M (2011) Prognostics of lithium-ion batteries based on Dempster–Shafer theory and the Bayesian Monte Carlo method. Journal of Power Sources 196(23): 10314–10321.

Hosen MS, Jaguemont J, Van Mierlo J and Berecibar M (2021) Battery lifetime prediction and performance assessment of different modeling approaches with consideration of temperature and discharge rate. iScience 24(3): 102060.

Hsieh M, Lin Y, Lee J and Chu K (2017) Acoustic emission analysis of lithium-ion battery electrode reactions for the battery state-of-charge estimation. International Journal of Electrochemical Science 12: 3246–3255.

Hsieh G, Lin JY and Li TH (2022) Piezoelectric-based acoustic emission monitoring with machine learning for internal short circuit detection in 20 Ah LFP cells. Journal of Power Sources 548: 232074.

Hu X, Feng F, Liu K, Zhang L, Xie J and Liu B (2019) State estimation for advanced battery management: Key challenges and future trends. Renewable and Sustainable Energy Reviews 114: 109334.

IEA (2024) Global EV Outlook 2024. Paris: International Energy Agency.

Liu Y, Zhao R, Sun J and Li W (2023) BMS alarm analysis and thermal event classification in large-scale electric bus fleets: Evidence from Shenzhen. Energy 268: 126741.

MEM (2022) Investigation Report on Electric Vehicle Battery Thermal Events (2021–2022). Beijing: Ministry of Emergency Management, People's Republic of China.

Mikolajczak C, Kahn M, White K and Long RT (2011) Lithium-Ion Batteries Hazard and Use Assessment. New York: Springer.

Peng C, Zhang J and Liu H (2024) Traction battery systems for railway applications: A technical review. IEEE Transactions on Transportation Electrification 10(1): 102–118.

Peters JF, Baumann M, Zimmermann B, Braun J and Weil M (2017) The environmental impact of Li-Ion batteries and the role of key parameters – A review. Renewable and Sustainable Energy Reviews 67: 491–506.

Peters JF, Peña Cruz A and Weil M (2019) Exploring the economic potential of sodium-ion batteries. Batteries 5(1): 10.

Ribiere P, Grugeon S, Morcrette M, Boyanov S, Laruelle S and Marlair G (2012) Investigation on the fire-induced hazards of Li-ion battery cells by fire calorimetry. Energy and Environmental Science 5(1): 5271–5280.

Romare M and Dahlöf L (2017) The Life Cycle Energy Consumption and Greenhouse Gas Emissions from Lithium-Ion Batteries. Stockholm: IVL Swedish Environmental Research Institute, Report C 243.

SBG (2021) Shenzhen Zero-Emission Bus Fleet Annual Report 2020. Shenzhen: Shenzhen Bus Group, Technical Report.

Schmalstieg J, Käbitz S, Ecker M and Sauer DU (2014) A holistic aging model for Li(NiMnCo)O_2 based 18650 lithium-ion batteries. Journal of Power Sources 257: 325–334.

Schmidt JP, Arnold S, Loges A, Werner D, Wetzel T and Ivers-Tiffée E (2013) Measurement of the internal cell temperature via impedance: Evaluation and application of a new method. Journal of Power Sources 243: 110–117.

Sihvo J, Mikkonen J and Repo T (2021) Automotive Li-ion cell state detection via broadband impedance spectra and a robust classifier. IEEE Transactions on Power Electronics 36(4): 4523–4534.

Vetter J, Novák P, Wagner MR, Veit C, Möller KC, Besenhard JO, Winter M, Wohlfahrt-Mehrens M, Vogler C and Hammouche A (2005) Ageing mechanisms in lithium-ion batteries. Journal of Power Sources 147(1–2): 269–281.

Waldmann T, Wilka M, Kasper M, Fleischhammer M and Wohlfahrt-Mehrens M (2014) Temperature dependent ageing mechanisms in Lithium-ion batteries – A Post-Mortem study. Journal of Power Sources 262: 129–135.

Yamazoe N, Sakai G and Shimanoe K (2003) Oxide semiconductor gas sensors. Catalysis Surveys from Asia 7: 63–75.

Zhang S, Zhao K, Zhu T and Li J (2017) Electrochemo-mechanical degradation of high-capacity battery electrode materials. Progress in Materials Science 89: 479–521.

Zhao Z, Hu Z, Fang Q and Zhai J (2023) Thermal management and temperature uniformity investigation of a prismatic lithium-ion battery module with the heat pipe thermal management system. Journal of Energy Storage 57: 106228.